Journal of Power Sources 194 (2009) 81–87

Contents lists available at ScienceDirect

Journal of Power Sources

journal homepage: www.elsevier.com/locate/jpowsour

Catalytically graphitized glass-like carbon examined as anode for lithium-ion cell performing at high charge/discharge rates

Jan M. Skowroński*, Krzysztof Knofczyński

Poznan University of Technology, Institute of Chemistry and Technical Electrochemistry, ul. Piotrowo 3, 60-965 Poznań, Poland

ARTICLE INFO

Article history:
Received 17 October 2008
Received in revised form 7 April 2009
Accepted 21 April 2009
Available online 3 May 2009

Keywords:
Spherical glass-like carbon
Catalytic graphitization
Lithium-ion cell
Anode
Intercalation
Insertion

ABSTRACT

The influence of a long-time heat treatment of hard carbon in the presence of iron catalyst on its structural properties and electrochemical performance is concerned in terms of potential application as anode material for lithium-ion cell. Glass-like carbon spheres obtained by carbonization of phenol resin were catalytically graphitized by heat treatment at temperature 1000 °C in argon atmosphere for 20 h and 100 h. After this process iron was completely removed from the product of reaction. The original carbon was entirely useless as anode for Li-ion cell because of its extremely poor reversible capacity (54 mAh g^{-1}). Due to heat treatment composite materials consisting of microcrystalline graphite admixed with turbostratic carbon were produced. Modified carbons were tested as anode materials using gradually increasing current density. Based on electrochemical measurements a mixed intercalation/insertion mechanism for storage of lithium ions was concluded. Discharge capacity of carbon heat treated for 100 h attained value of 276 mAh g^{-1} and its reversible capacity appeared to be better than that of flaky graphite upon discharging at current density in the range 50–250 mA g^{-1}.

1. Introduction

There are many types of carbon materials for various applications, from bike, car, yachting, military, cosmic industry to primary and secondary cells [1–3]. With the exception of natural carbon materials (e.g., graphite), artificial carbons are usually produced by heat treatment of organic precursors in the temperature range from 650 °C to 3000 °C in an inert atmosphere. The basic unit of all carbon materials is graphene sheet [4–6]. From structural point of view, three groups of carbon materials can be used as anode for lithium-ion cells: graphites, soft and hard carbons [4]. Graphite consists of parallel graphene layers with $AB(AB)_n$ sequence (in the hexagonal structure) [4–6]. Graphite can be divided into two classes: (i) natural micro- or macrocrystalline graphite (found as mineral in earth) and (ii) synthetic graphite obtained by the high temperature treatment of raw material, usually around 3000 °C [7]. Soft carbons (graphitizable carbons) can easily be converted into graphite. Typical precursor for soft carbons is petroleum coke [4,7]. Hard carbons (non-graphitizable carbons) cannot be converted into crystalline structure of graphite under ambient pressure due to high temperature treatment even at temperature 3000 °C. Thermosetting polymers (e.g., phenolic resin) or vegetable fibers (e.g., coconut shell or cedar tree [8]) are commonly used as precursors of hard carbon [4,7]. Soft and hard carbons prepared at low temperatures (below 1000 °C) consist of graphene layers which, contrary to graphite, are unparallel to each other and have "house of cards" structure [4,7,8]. Turbostratic phase (typical component of hard carbons treated at high temperature) can be described as a short–long range stacking of graphene layers with larger distance between graphene layers (close to 0.34 nm) as compared to graphite [4], and without perfectly periodical $AB(AB)_n$ sequence of graphene layers (e.g., chaotic stacking ADBBAC, etc.) [8,9].

A successful graphitization of hard carbons into graphite structure is possible using special conditions of heat treatment, such as: (i) high pressure [10] and (ii) presence of catalyst such as iron and iron oxides [11–17], inorganic and organic compounds of iron (e.g, iron(III) nitrate [18] and iron(III) acetylacetonate [19,20]) undergoing thermal decomposition to iron oxides followed by metallic iron. Nickel [21,22] and nickel(III) compounds [23] were also used for catalytic graphitization. During graphitization of both soft and hard carbons the following changes in crystalline structure occur on increasing the temperature in the range 650–3000 °C: precursor → graphene sheets initiation → "house of cards" structure → turbostratic phase → artificial graphite. There is some controversy concerning the susceptibility of carbon black to graphitization. Kinoshita and Zaghib [24] regarded carbon black as an example of soft carbon, whereas Song and co-workers [18] claimed that carbon black, belonging to the class of non-graphitizable carbons, can be converted to graphite provided the process of graphitization is catalytically assisted. The transforma-

* Corresponding author. Tel.: +48 616653641; fax: +48 616652571.
E-mail address: jan.skowronski@put.poznan.pl (J.M. Skowroński).

0378-7753/$ – see front matter © 2009 Published by Elsevier B.V.
doi:10.1016/j.jpowsour.2009.04.048

tion of acetylene carbon black into graphite structure can occur at 1000 °C in a mixture with $Fe(NO_3)_3 \cdot 9H_2O$ [18]. This compound undergoes decomposition to Fe_2O_3 during heat treatment, and then is reduced by carbon to the final catalytic form of metallic iron. The authors of Ref. [18] suggested that during a three-step process: (i) the metal–carbon solid solution is formed and (ii) carbon dissolves in iron to supersaturation, (iii) carbon reprecipitates step by step from semi-solid solution to form graphite during supersaturation or cooling down. Catalytic effect of iron oxide in the graphitization process of hard carbon/soft carbon composite during heat treatment at 2500 °C was investigated by Mathur and co-workers [25]. While the product did not reached the completely perfect ordering in this process, the structure of sample was improved. A higher ordering of the composite structure was attributed to the formation of iron carbide (above 1400 °C), which dissociated to graphitic carbon and iron after attaining the melting point at around 1550–1600 °C. The process of graphitization of hard carbons during HTT at distinctly lower temperature of 1000 °C with assistance of iron powder as catalyst was presented elsewhere [11,12].

Carbon materials have ability to reversible storage of lithium ions inside their structure [4,5,26–32]. Two kinds of mechanisms are usually concerned: (i) intercalation/deintercalation with the occurrence of so-called "staging phenomenon" occurring and (ii) insertion/deinsertion one. According to the first mechanism taking place for graphite and graphite-like materials, lithium ions are located between graphene layers. The second mechanism referring to unorganized carbons (involving hard carbons) assumes that lithium ions are accumulated in pores and structural defects of carbon material, formed by unparallel stacking of graphene layers. The maximum theoretical reversible capacity for graphite of 372 mAh g^{-1} corresponds to graphite intercalation compound (GIC) with the composition LiC_6 [5,26,27]. Non-graphitizable carbons are not under this rule, and reversible capacities for these materials (measured in the second and the following cycles) are mostly higher than that for graphite. Unfortunately, a very large irreversible capacity for the first cycle is a serious disadvantage. Practical values of reversible capacities of hard carbons depend on many factors, e.g., type of precursor, temperature of heat treatment, presence of heteroatoms in carbon matrix. Irreversible capacity, defined as a difference between electric charge consumed by carbon electrode during the process of intercalation/insertion and the charge recovered during the process of deintercalation/deinsertion (reversible capacity), is connected with (i) the reaction of lithium ions with surface functional groups of carbon materials, (ii) the decomposition of electrolyte's solvent followed by the formation of passive surface film (so-called solid electrolyte interface, SEI) [33–39], (iii) the reaction of lithium ions with water present in carbon sample, and (iv) irreversible intercalation or insertion of lithium ions.

In this work, a long-time catalytically assisted graphitization was investigated. As shown, the reaction solid-state between hard carbon and catalyst occurred at a temperature around 500 °C lower than the melting point of iron. The XRD analysis data supported by the cyclic voltammetry (CV) and galvanostatic methods proved clearly the conversion of non-graphitizable carbon into graphite slightly admixed with turbostratic carbon. The obtained graphite/turbostratic carbon composite exhibited better electrochemical usefulness for practical application as anode for lithium-ion cell in comparison with both the completely unorganized original glass-like carbon and flaky graphite.

2. Experimental

Spherical glassy-like carbon, as commercial product of Owada Carbon Ltd., was used as starting material (denoted as GP-30). This carbon was produced from a phenolic resin by thermal treatment up to 1000 °C in a nitrogen atmosphere. The SEM observations showed this material (Fig. 1) to be composed of carbon spheres ranging mostly in diameters around 10–15 μm [11]. Physicochemical data gathered for the original carbon (sample GP-30), sample GP-30 heat treated at 2700 °C and the product obtained by heat treatment of sample GP-30 at 1000 °C in a mixture with iron powder for 4 h in argon were presented earlier [11]. In this work, the following modifications of the starting carbon GP-30 were done: (i) heat treatment at 1000 °C in a mixture with iron powder for 20 h (sample denoted as GP-30/1000-20/Fe) and (ii) heat treatment at 1000 °C in a mixture with iron particles for 100 h (sample denoted as GP-30/1000-100/Fe). Iron powder (Merck, iron content >99.5 wt.%) was composed of grains 1–5 μm in diameter. The weight ratio of carbon to iron in the mixture was 1:11 (a volume ratio ca. 1:3). Carbons were heat treated in a pipe furnace (quartz glass pipe) in the stream of argon. After cooling down to ambient temperature the sintered carbon/iron product was treated with diluted HCl solution to remove any metallic components. Then the modified carbon was washed out with distilled water until chloride ions disappeared in a filtrate. All the samples were characterized using XRD analysis ((PW-1710, Philips), Cu Kα radiation). Scanning electron microscopy (SEM; Tescan–Vega 5135) coupled with the energy dispersive X-ray (EDS; PGT—Princeton Gamma Tech) analysis was used for observing the changes in microstructure and to verify the complete removal of iron from modified carbons. High-resolution transmission electron microscopy (HRTEM; FEI Tecnai G2 F20 S Twin) was used for observing the changes in the local microstructure of the graphitized carbons.

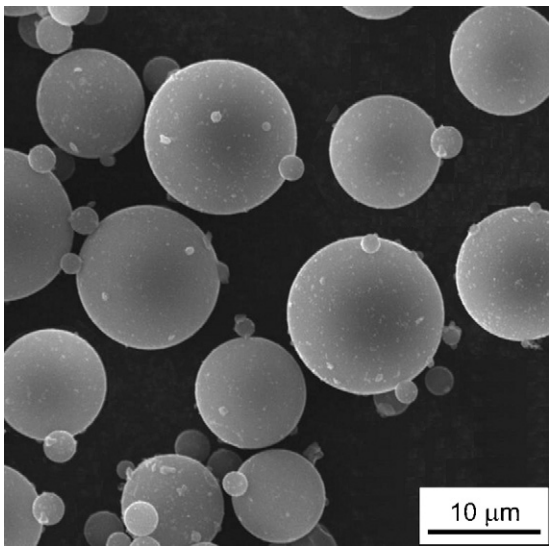

Fig. 1. SEM micrograph for the original carbon (sample GP-30).

The working electrodes for electrochemical measurements were prepared by mixing carbon powder (85 wt.%) with poly(vinylidene fluoride) (PVDF) (15 wt.%) as a binder dissolved in 1-methyl-2-pyrrolidone. The carbon/binder/solvent pulp was spread on nickel net, dried at 120 °C in vacuum. After this, the electrodes were dried again at 120 °C for 12 h under vacuum and without contact with atmosphere safely transferred to a dried glove-box filled with dry argon and mounted in the coin-type half-cell (CR 2430). The electrode diameter was 1.75 cm, whereas the weight of carbon/PVDF material in the electrode was around 20 mg. The counter and reference electrodes were made of lithium foil, a microporous polypropylene separator was inserted between the carbon working electrode and counter lithium electrode [8,11,12]. The electrolyte was 1 M $LiPF_6$ dissolved in a mixture of ethylene carbonate (EC) and diethyl carbonate (DEC) (1:1 by weight). The XRD and electrochemical measurements were performed for electrodes made

of the original carbon, carbons modified by catalytic heat treatment and flaky graphite donated by Carbon Lorraine (particles of spectroscopic graphite with diameters smaller than 25 μm). Electrochemical measurements were performed using ATLAS 9835 v. 5V2A Sollich for galvanostatic mode and PAR 273A, EG&G for cyclic voltammetric mode. The specific capacity of the carbon electrode was measured by the galvanostatic charge (lithium intercalation/insertion)/discharge (lithium deintercalation/deinsertion) method by cycling in the potential range 0–2.5 V, using for the first charge/discharge cycle a current density of 30 mA g^{-1} of active substance. Upon starting the galvanostatic measurements, the carbon electrode was cathodically reduced (charged). For comparison, galvanostatic curves for anodes made of samples GP-30/1000-20/Fe, GP-30/1000-100/Fe and flaky graphite were presented in a shortened potential range of 0.25–0 V. In addition, the influence of current density on the electrochemical behaviour of all the carbon anodes was determined. Two galvanostatic cycles were carried out for each current density, which was changed in the following order: 30 mA g^{-1}, 50 mA g^{-1}, 100 mA g^{-1}, 150 mA g^{-1}, 200 mA g^{-1} and 250 mA g^{-1}. These numbers corresponded to current densities 0.21 mA cm^{-2}, 0.35 mA cm^{-2}, 0.70 mA cm^{-2}, 1.05 mA cm^{-2}, 1.40 mA cm^{-2} and 1.75 mA cm^{-2}, respectively. CV measurements, with a scan rate of 0.01 mV s^{-1}, were carried out in the potential range 0–2.5 V, starting in the negative direction of the potentials. The potentials in this paper are quoted against a Li/Li^+ electrode. All electrochemical measurements were performed at a temperature of 20 °C.

3. Results and discussion

3.1. Morphology and structure of carbons

The SEM image for the original carbon (Fig. 1) shows this material to be composed of smooth spheres ranging mostly in diameters around 10–15 μm. Figs. 2 and 3 allow the illustration of the influence of the catalytically assisted heat treatment on the morphology of carbons. As can be seen from these figures, the original spheres of sample GP-30 are destroyed due to heat treatment. Fig. 2 shows the product of 20 h heat treatment composed of two kinds of spheres. The first group involves spheres with many small pinholes on their surface, whereas spheres of the second group are badly pitted or even transformed into cup-like bodies. The product of 100 h heat

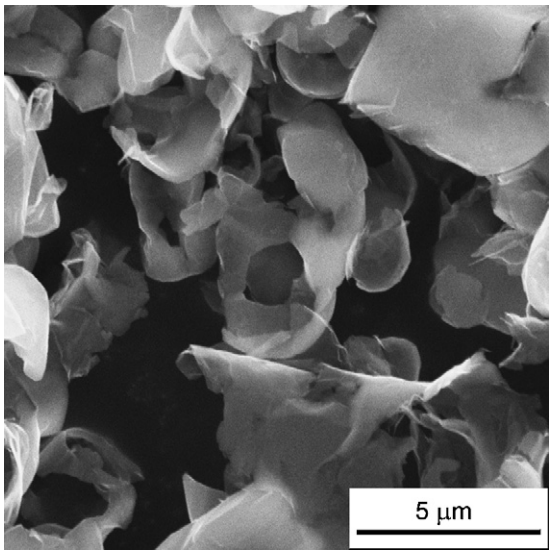

Fig. 3. SEM micrograph for carbon after HTT in the presence of catalyst (sample GP-30/1000-100/Fe).

treatment (Fig. 3) consists of the arch-like shells of different curvature and thickness around 50–150 nm. Disregarding their curved form, they are quite similar to the flat graphite flakes. Taking into account this result, it is reasonable to infer that hard carbon spheres of sample GP-30 were effectively transformed into more or less curved graphite-like flakes.

The HRTEM analyses were carried out to get a deeper insight into the microstructure of graphitized samples. The HRTEM images were taken in numerous regions of the samples and those shown in Figs. 4 and 5 are representative of the whole of the sample. Three microstructures were found for sample GP-30/1000-20/Fe obtained during 20 h of graphitization (Fig. 4). The outer region is built of the graphite coating composed of 8–15 graphene layers. The inferior local ordering and the presence of turbostratic graphite are found under this shell. In addition, residual phase of unorganized carbon is encapsulated within the graphitic and turbostratic phases. After 100 h of catalytic treatment the core–shell effect is not observed, the original phase of unorganized carbon completely disappears, while structural ordering increases (Fig. 5). As a consequence, sam-

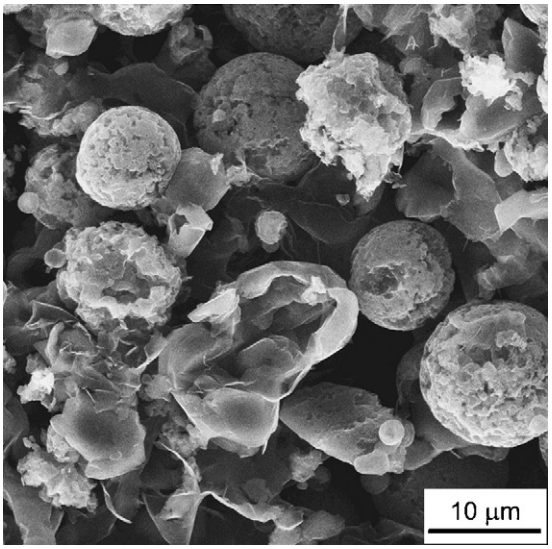

Fig. 2. SEM micrograph for carbon after HTT in the presence of catalyst (sample GP-30/1000-20/Fe).

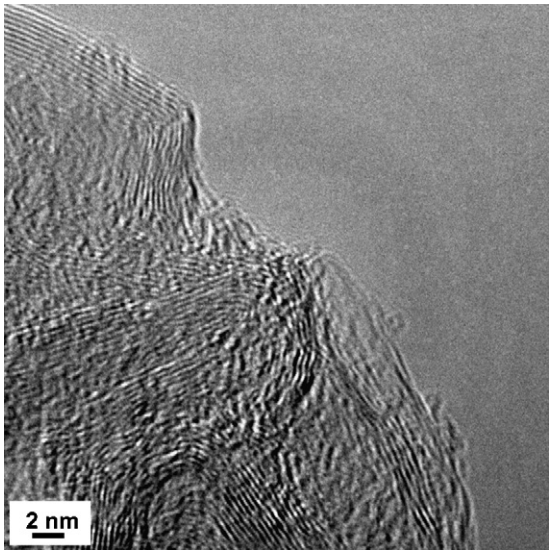

Fig. 4. HRTEM micrograph for carbon after HTT in the presence of catalyst (sample GP-30/1000-20/Fe).

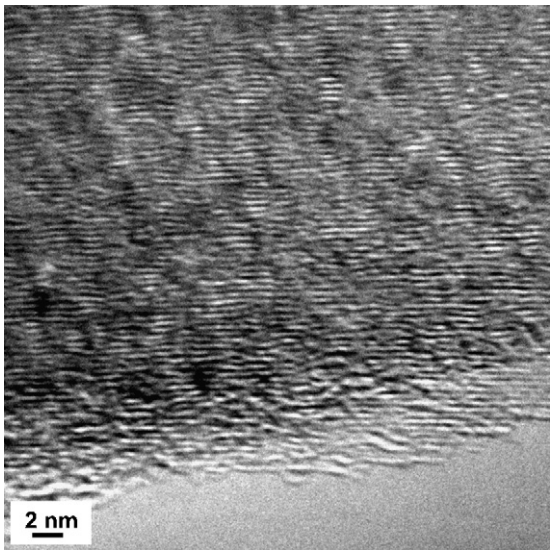

Fig. 5. HRTEM micrograph for carbon after HTT in the presence of catalyst (sample GP-30/1000-100/Fe).

ple GP-30/1000-100/Fe is homogeneous mixture of graphitic and turbostratic microstructures.

The XRD patterns recorded for the examined samples (Fig. 6), being in a good consistency with the SEM and HRTEM observations, allow the conclusion that samples GP-30/1000-20/Fe and GP-30/1000-100/Fe contain graphitic phase with AB(AB)$_n$ sequence characteristic of hexagonal structure of graphite. On the XRD pattern recorded for sample GP-30 no sharp peaks are observed (Fig. 6a). Instead, two broad waves at about 23° (2Θ) and 44° (2Θ) are noted (Table 1). This feature proves the original carbon to be structurally unorganized. As reported earlier [11], after heat treatment at 2700 °C the crystalline structure of sample GP-30 was only slightly improved. Its degree of crystallinity remained very far from the graphite structure. No diffraction peak characteristics of graphite were observed, except a traced (0 0 2) peak, being at early stage of formation. This result confirms that sample GP-30 produced from a phenolic resin belongs to the class of hard carbons. Fig. 6b and c presents the XRD patterns recorded for samples GP-30/1000-20/Fe and GP-30/1000-100/Fe obtained by heat treatment in the presence of iron catalyst for 20 h and 100 h, respectively. The EDS analysis carried out for these carbons revealed the presence of neither iron nor iron compounds. Table 1 gathers the structural data for examined carbons together with those for flaky graphite. The presence of graphite phase in carbons obtained due to catalytic heat treatment is evidenced by XRD patterns (Fig. 6b and c), where sharp (0 0 2) and (0 0 4) diffraction peaks of graphite are observed together with (1 0 0) and (1 0 1) peaks, characteristic of a three-dimensional structure of graphite [5,32].

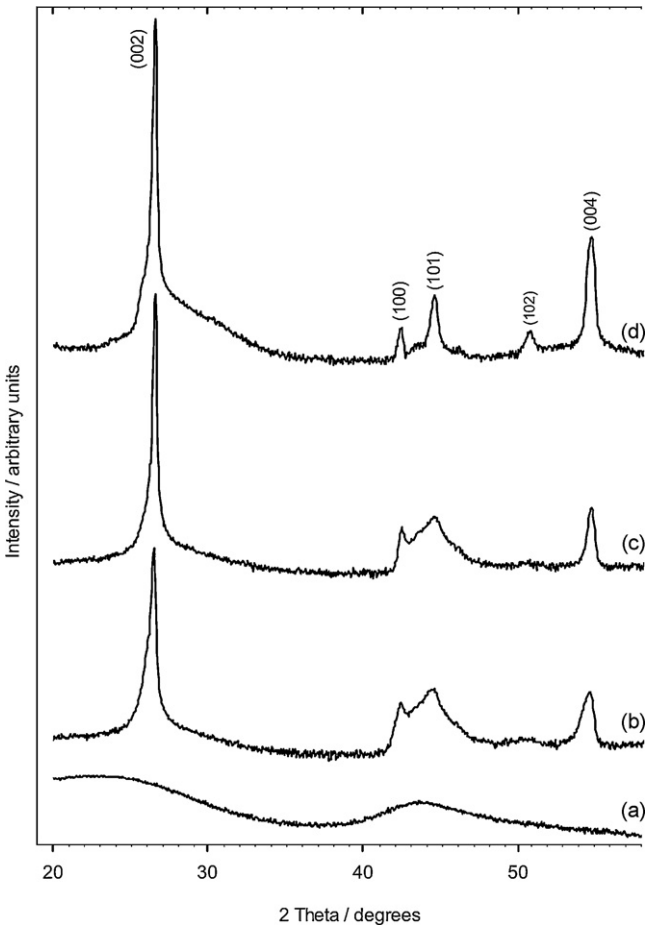

Fig. 6. Comparison of XRD patterns for (a) the original carbon (sample GP-30), (b) sample GP-30 after 20 h of catalytic heat treatment at 1000 °C, (c) sample GP-30 after 100 h of catalytic heat treatment at 1000 °C, and (d) flaky graphite. Cu Kα radiation.

The prolongation of catalytic heat treatment of sample GP-30 from 20 h to 100 h resulted in the enhancement of crystalline ordering of obtained sample GP-30/1000-100/Fe in comparison with sample GP-30/1000-20/Fe. As seen in Table 1, all four parameters were improved significantly: smaller full width at half-maximum (FWHM) of the (0 0 2) peak as well as interlayer spacing ($d_{(002)}$), larger crystallite dimensions along *c*-axis (L_c) and *a*-axis (L_a). The values of $d_{(002)}$ for samples GP-30/1000-20/Fe and GP-30/1000-100/Fe are very similar, whereas the values of L_a and L_c are distinctly smaller in comparison with flaky graphite. Almost symmetrical and narrow peaks (0 0 2) and (0 0 4) seen on the XRD pattern recorded for sample GP-30/1000-100/Fe suggests graphene layers to be parallel to each other, whereas the presence of the (1 0 0) and (1 0 1) peaks indicates that graphene layers tend to stack in the AB(AB)$_n$ sequence, similar to flaky graphite [32]. The latter peaks are, however, unsymmetrical and not fully separated (Fig. 6c), as compared to those for flaky graphite (Fig. 6d). This feature can be attributed to the admixture of turbostratic carbon to the graphitic phase. According to data reported in Ref. [32], carbon material can be regarded as microcrystalline graphite if the value of L_a is below 1000 nm, and for such a material the (1 0 0) and (1 0 1) peaks can be unseparated. Sample GP-30/1000-100/Fe with the L_a value of 320 nm well matches this criterion. The results of structural examinations using the HRTEM and XRD techniques lead to the conclusion that due to catalytically assisted heat treatment of glass-like carbon for 100 h unorganized hard carbon spheres are transformed into microcrystalline graphite admixed with turbostratic carbon at temperature considerably lower than temperatures used for a standard process of graphitization (around 3000 °C). The mechanism of catalytic graphitization for the glass-like carbon spheres/iron catalyst system has been considered in our previous papers [11,12].

3.2. Electrochemical behaviour of carbons

Sample GP-30 exhibits electrochemical properties entirely useless for practical application in lithium-ion cells, because for the first cycle measured under current density of 30 mA g^{-1} its irreversible capacity of 73 mAh g^{-1} is higher than reversible capacity and, moreover, reversible capacity of 54 mAh g^{-1} is extremely low. In comparison with sample GP-30, both carbons obtained by catalytic graphitization demonstrate comparable irreversible capacities (close to that of flaky graphite) and their reversible capac-

Table 1
XRD data for examined carbons.

Sample	Structural parameters			
	Full width at half-maximum of the (0 0 2) peak (°, 2θ)	Interlayer spacing $d_{(002)}$ (nm)	Crystallite size	
			L_c (nm)	L_a (nm)
GP-30	9.158	–	–	–
GP-30/1000-20/Fe	0.399	0.3374	300	155
GP-30/1000-100/Fe	0.286	0.3357	500	320
Flaky graphite	0.240	0.3352	9070	835

Table 2
Electrochemical parameters of examined electrodes calculated from the first charge/discharge cycle (current density 30 mA g^{-1}).

Sample	Reversible capacity, Q_R (mAh g^{-1})	Irreversible capacity, Q_{IR} (mAh g^{-1})	Total charge capacity ($Q_R + Q_{IR}$) (mAh g^{-1})	First cycle discharge/charge efficiency, $Q_R/(Q_R + Q_{IR})$ (%)
GP-30	54	73	127	43
GP-30/1000-20/Fe	274	81	355	77
GP-30/1000-100/Fe	276	74	350	79
Flaky graphite	334	80	414	81

ities around 275 mAh g^{-1} are a fivefold higher (Table 2, Fig. 7). The highest reversible capacity of 334 mAh g^{-1}, obtained at the same charge/discharge current density, is noted for the flaky graphite electrode. In the first cycle carried out under current density of 30 mA g^{-1} samples GP-30/1000-20/Fe and GP-30/1000-20/Fe demonstrate almost the same reversible capacities. As can be seen in Fig. 7, before intercalation of lithium ions, occurring below the potential of 0.25 V, the potential plateau associated with the formation of SEI appears at about 0.8 V [12,24,29,37]. The charge related to SEI is irretrievably lost and cannot be recovered during the anodic discharge of carbon electrode.

In Fig. 8a–d enlarged sections of Fig. 7 are presented in the potential range from 0.25 V to 0 V. Several potential plateaux, arising from the staging phenomenon, are observed on curve related to flaky graphite (Fig. 8a). This phenomenon is a characteristic feature of the intercalation/deintercalation process consisting in a successive filling of the interlayer spacings of graphite with intercalate (lithium ions) [5,27,29]. A lack of any plateaux is typical for non-graphitic materials, e.g., low-temperature hard carbons (Fig. 8b). In Fig. 8c, obtained for sample GP-30/1000-20/Fe, such

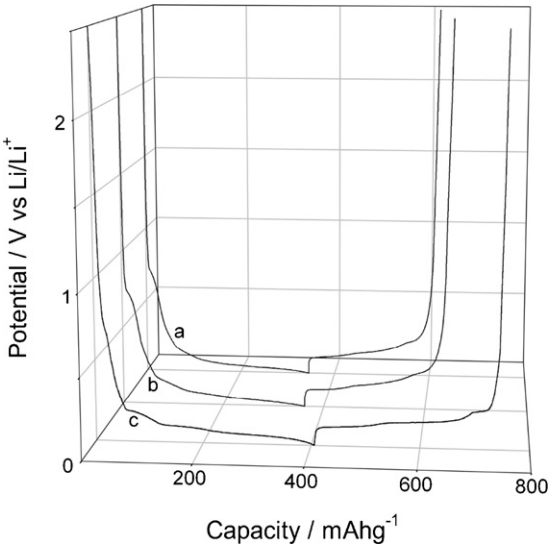

Fig. 7. Galvanostatic curves recorded during the first charge/discharge cycle in the potential range from 2.5 V to 0 V for: (a) sample GP-30/1000-20/Fe, (b) sample GP-30/1000-100/Fe (1:11), and (c) flaky graphite. Current density of 30 mA g^{-1}.

plateaux are barely visible, whereas in Fig. 8d, recorded for sample GP-30/1000-100/Fe, these plateaux are much better distinguishable. This improvement can be ascribed to the complete decay of amorphous phase and enrichment of sample GP-30/1000-100/Fe in graphite phase due to a fivefold longer process of graphitization. The plateaux recorded for this sample are slightly worse pronounced in comparison to those observed for flaky graphite (Fig. 8a). In agreement with the HRTEM and XRD data, such an observation can be related to turbostratic carbon still admixing the graphite phase. While the XRD pattern supported by the appearance of the potential plateaux recorded on the galvanostatic curve is evidence for the creation of hexagonal graphite structure in sample GP-30/1000-100/Fe, turbostratic carbon remaining in the graphite matrix makes the charge/discharge process to occur according to a mixed intercalation/insertion mechanism.

Concerning reversible capacities noted for the second cycle under current density of 30 mA g^{-1} (Fig. 9), one can notice that the flaky graphite electrode is still the best one, whereas the electrode prepared using sample GP-30/1000-100/Fe behaves better than that prepared using sample GP-30/1000-20/Fe. Flaky graphite demonstrates the highest reversible capacity both in the first and second cycle only under the lowest current density of 30 mA g^{-1}. For all the higher current densities, carbon GP-30/1000-100/Fe exhibits better reversible capacities not only in comparison with sample GP-30/1000-20/Fe but also with flaky graphite. This result is promising from a point of view of practical application of catalytically graphitized hard carbons for lithium-ion cells performing under high-rate conditions. A better galvanostatic performance of sample GP-30/1000-100/Fe in comparison with that heat treated for a fivefold shorter time can be explained in terms of structural properties. Sample GP-30/1000-100/Fe has a higher crystallite dimension and smaller interlayer spacing $d_{(002)}$ (Table 1, Fig. 6). The latter feature may be related to both the lack of unorganized carbon and lower content of turbostratic phase in this sample. It seems likely that the ratio of graphite phase to turbostratic carbon, giving rise to the improvement of anode performance under a high-rate discharge [4,24,32], is favorably matched to a good rate capability of sample GP-30/1000-100/Fe. A higher reversible capacity of sample GP-30/1000-100/Fe than that of flaky graphite, noted on increasing current density in the range 50–250 mA g^{-1}, can be explained by a local isotropic behaviour of graphitized sample. Such a behaviour is characteristic of microcrystalline graphite [32]. Owing to the existence of isotropic domains in graphite matrix the mechanical stability and integrity of electrodes is enhanced during many

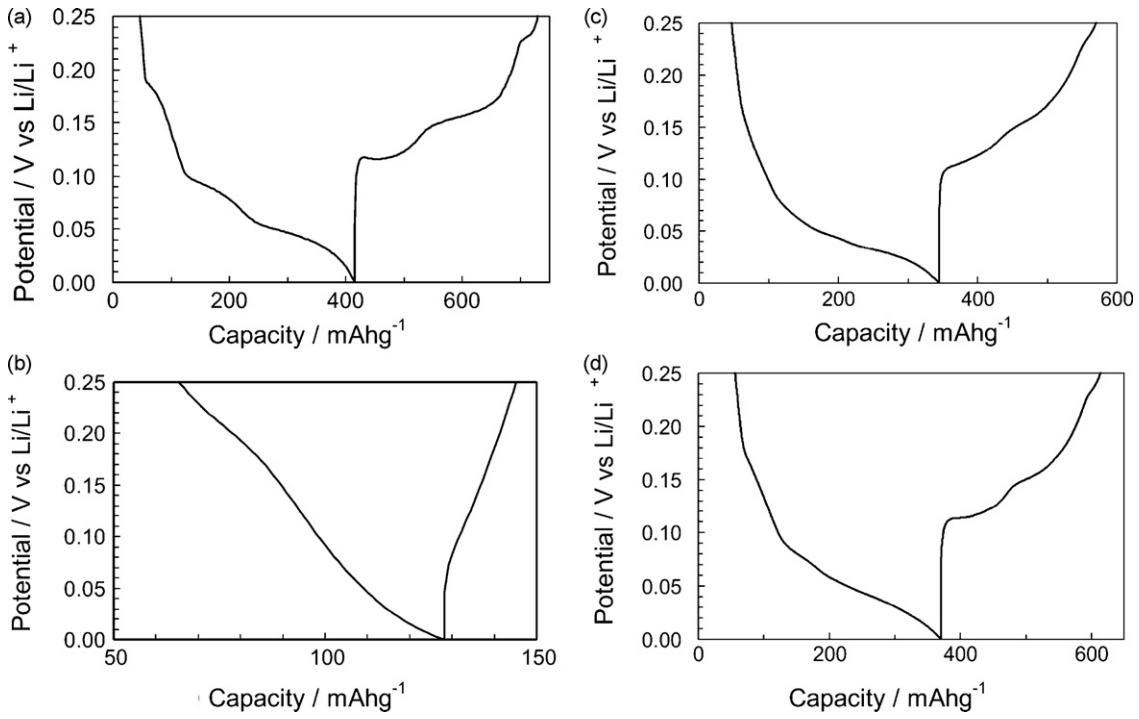

Fig. 8. Galvanostatic curves recorded during the first charge/discharge cycle in the potential range from 0.25 V to 0 V for (a) flaky graphite, (b) sample GP-30, (c) sample GP-30/1000-20/Fe, and (d) sample GP-30/1000-100/Fe. Current density of 30 mA g^{-1}.

consecutive charge/discharge cycles, especially at a high current density.

Fig. 10 presents CV curves recorded for sample GP-30/1000-20/Fe. The cathodic peak appearing only for the first cycle at the potential of 752 mV is associated with irreversible reaction of the formation of SEI. Similar cathodic peak is noted at the potential of 784 mV for sample GP-30/1000-100/Fe (Fig. 11). The potentials of these peaks are in a good consistence with the potential plateau recorded galvanostatically during the first charge run (Fig. 7). The cathodic peaks recorded for both samples during the first and second cycle in the range from 250 mV to 0 mV are connected with intercalation of lithium ions into graphite phase (Figs. 10 and 11). The sequence of three anodic peaks recorded during the second cycle for sample GP-30/1000-20/Fe at the potentials of 152 mV, 192 mV, and 244 mV represent the process of deintercalation of lithium ions from the interlayer spacings of graphite, according to the staging phenomenon. These peaks are not completely separated (Fig. 10). On the contrary to sample GP-30/1000-20/Fe, the anodic peaks of deintercalation recorded at the potentials of 136 mV, 178 mV, and 240 mV during the second cycle of sample GP-30/1000-100/Fe are narrower and almost completely separated (Fig. 11). Such a behaviour may be accounted for by enhanced deintercalation of lithium ions as result of a better structural ordering of sample heat treated for 100 h, as compared to sample heat treated for a fivefold shorter time. The reason for not perfectly separated peaks for both modified glass-like carbons may be related to the coexistence of turbostratic carbon concluded based on the afore-discussed galvanostatic curves. On the other hand, the best kinetics of the intercalation/deintercalation process for sample GP-30/1000-100/Fe representing the graphite/turbostratic carbon ratio matched better than that for sample GP-30/1000-20/Fe, can be recognized as the reason for the lowest loss of capacity under the

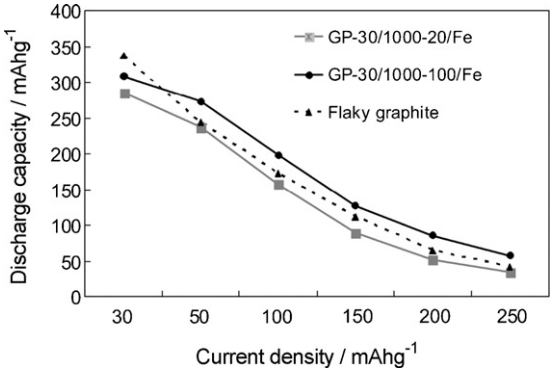

Fig. 9. Comparison of discharge capacities for samples examined under increasing current density. The second cycles are presented for each current density.

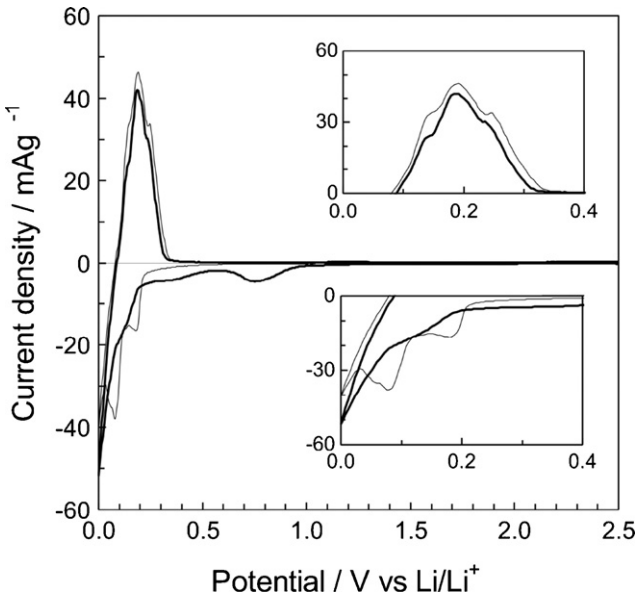

Fig. 10. Cyclic voltammograms recorded for sample GP-30/1000-20/Fe, (—) cycle 1, (—) cycle 2. Scan rate 0.01 mV s^{-1}.

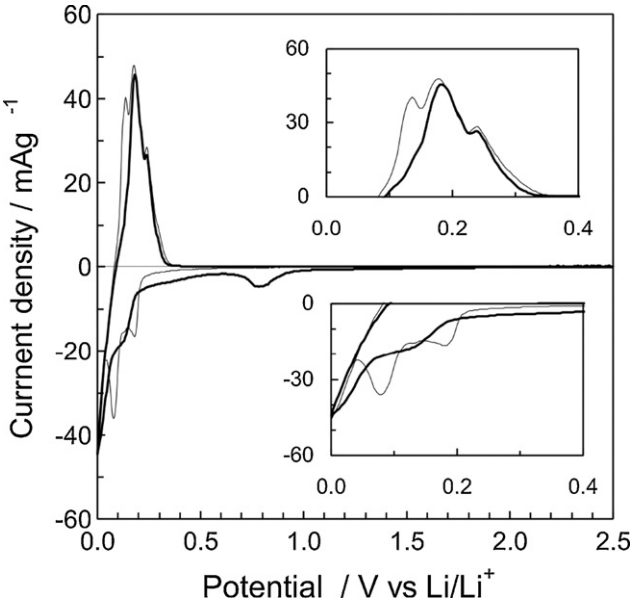

Fig. 11. Cyclic voltammograms recorded for sample GP-30/1000-100/Fe, (—) cycle 1, (—) cycle 2. Scan rate 0.01 mV s^{-1}.

cyclic high-rate charge/discharge performance. An assumption that the presence of turbostratic disordered carbon facilitates faster transport of lithium ions allows also the elucidation of a better performance of sample GP-30/1000-100/Fe in comparison with flaky graphite.

4. Conclusions

Experimental data obtained by the XRD analysis and the CV and galvanostatic measurements clearly proved successful transformation of hard carbon spheres into a hybrid composite composed of hexagonal graphite phase admixed with turbostratic carbon due to heat treatment of a glass-like carbon in a mixture with iron catalyst. The time of this process played an important role in this process. The material heat treated for 100 h tested as possible anode for lithium-ion cell at current densities in the range from 50 mA g^{-1} to 250 mA g^{-1} appeared to be better even as compared to flaky graphite. In this range of current density the discharge capacity of sample GP-30/1000-100/Fe is about 15% higher than that of flaky graphite. The coexistence of graphite phase and the turbostratic disordered carbon present in this composite is likely essential for a good performance of anode under the high-rate charge/discharge. The proposed method of graphitization offers a simple and attractive way in searching for composite-type carbon materials demonstrating structural and physical properties potentially useful for practical application in the high-rate lithium-ion cells.

Acknowledgement

The authors gratefully acknowledge Dr. hab. E. Borowiak-Palen (the West Pomeranian University of Technology, Szczecin) for the HRTEM images.

References

[1] J.P. Fellner, G.J. Loeber, S.P. Vukson, C.A. Riepenhoff, J. Power Sources 119–121 (2003) 911–913.
[2] A.G. Ritchie, J. Power Sources 136 (2004) 285–289.
[3] R. Gitzendanner, F. Puglia, C. Martin, D. Carmen, E. Jones, S. Eaves, J. Power Sources 136 (2004) 416–418.
[4] H. Azuma, H. Imoto, S. Yamada, K. Sekai, J. Power Sources 81–82 (1999) 1–7.
[5] J.M. Skowroński, in: H.S. Nalva (Ed.), Handbook of Organic Conductive Molecules and Polymers, vol. 1, Wiley and Sons, Chichester, 1997, pp. 621–686.
[6] B. Kwiecińska, H.I. Petersen, Int. J. Coal Geol. 57 (2004) 99–116.
[7] M. Wissler, J. Power Sources 156 (2006) 142–150.
[8] J.M. Skowroński, K. Knofczyński, Y. Yamada, Solid State Ionics 157 (2003) 133–138.
[9] L. Tirado, Mater. Sci. Eng. R40 (2003) 103–136.
[10] X. Wang, G.M. Zhang, Y.L. Zhang, F.Y. Li, R.C. Yu, C.Q. Jin, G.T. Zou, Carbon 41 (2003) 188–191.
[11] J.M. Skowroński, K. Knofczyński, J. New Mater. Electrochem. Syst. 9 (2006) 359–365.
[12] J.M. Skowroński, K. Knofczyński, M. Inagaki, Solid State Ionics 178 (2007) 137–144.
[13] M. Inagaki, K. Fujita, Y. Takeuchi, K. Osada, H. Iwata, H. Konno, Carbon 39 (2001) 921–929.
[14] M. Inagaki, Y. Okada, H. Miura, H. Konno, Carbon 37 (1999) 329–334.
[15] A. Oberlin, J.P. Rouchy, Carbon 9 (1971) 39–46.
[16] Y. Hishiyama, A. Ono, T. Tsuzuku, Carbon 6 (1968) 203–208.
[17] A. Oya, H. Marsh, J. Mater. Sci. 17 (1982) 309–322.
[18] W. Lian, H. Song, X. Chen, L. Li, J. Huo, M. Zhao, G. Wang, Carbon 46 (2008) 525–530.
[19] S.H. Park, S.M. Jo, D.Y. Kim, W.S. Lee, B.C. Kim, Synth. Met. 150 (2005) 265–270.
[20] S.E. Hong, D.-K. Kim, S.M. Jo, D.Y. Kim, B.D. Chin, D.W. Lee, Catal. Today 120 (2007) 413–419.
[21] S.-S. Tzeng, Carbon 44 (2006) 1986–1993.
[22] S.-S. Tzeng, Y.H. Lin, Carbon 46 (2008) 555–558.
[23] X. Wang, J. Liu, Z. Li, J. Non-Crystal. Solids 355 (2009) 72–75.
[24] K. Kinoshita, K. Zaghib, J. Power Sources 110 (2002) 416–423.
[25] S.R. Dhakate, R.B. Mathur, O.P. Bahl, Carbon 35 (1997) 1753–1756.
[26] N. Imanishi, Y. Takeda, O. Yamamoto, in: M. Wakihara, O. Yamamoto (Eds.), Lithium Ion Batteries, Kodansha/Wiley-VCH, Tokyo/Weinheim, 1998, pp. 98–126.
[27] M. Winter, J.O. Besenhard, in: J.O. Besenhard (Ed.), Handbook of Battery Materials, Wiley-VCH, Weinheim, 1999, pp. 383–418.
[28] M. Endo, C. Kim, K. Nishimura, T. Fujino, K. Miyashita, Carbon 38 (2000) 183–197.
[29] S. Flandrois, B. Simon, Carbon 37 (1999) 165–180.
[30] E. Buiel, J.R. Dahn, Electrochim. Acta 45 (1999) 121–130.
[31] J.M. Skowroński, K. Knofczyński, S. Błażewicz, Synth. Met. 135–136 (2003) 733–734.
[32] L. Zou, F. Kang, X. Li, Y.-P. Zheng, W. Shen, J. Zhang, J. Phys. Chem. Solids 69 (2008) 1265–1271.
[33] A. Roger, E. Peled, E. Gileadi, J. Electrochem. Soc. 123 (1976) 638–642.
[34] E. Peled, J. Electrochem. Soc. 126 (1979) 2047–2051.
[35] E. Peled, D. Golodnitsky, J. Pencier, in: J.O. Besenhard (Ed.), Handbook of Battery Materials, Wiley-VCH, Weinheim, 1999, pp. 419–456.
[36] K. Zaghib, R. Yazami, M. Broussely, J. Power Sources 68 (1997) 239–241.
[37] R. Yazami, M. Deschamps, F. Genies, J.C. Frison, J. Power Sources 68 (1997) 110–113.
[38] R. Yazami, Electrochim. Acta 45 (1999) 87–97.
[39] D. Aurbach, B. Markovsky, I. Weissman, E. Levi, Y. Ein-Eli, Electrochim. Acta 45 (1999) 67–86.